A Very-Low-Q Diffractometer for an Advanced Spallation Source

Philip A. Seeger and Rex P. Hjelm, LANSCE, Los Alamos National Laboratory
Los Alamos, NM 87544-1663, USA

Abstract

Proposals to build new, more powerful spallation sources and the introduction of advanced moderator concepts will result in neutron sources that are 20 times more luminous than the brightest available today. These developments provide opportunity and challenge to expand the capabilities of present low-Q instruments using new designs. A particularly interesting case is the design of an instrument capable of measurements to "very low" momentum transfer, say $Q \approx 0.0007$ Å^{-1}. We consider an instrument to be built on a 20 Hz, 330 kW target and viewing a coupled liquid-hydrogen moderator. The instrument would use a frame-definition chopper to select a wavelength band suitable for the required Q-domain. Monte Carlo optimization of the geometry was performed by choosing the minimum observable Q always to be 0.0007 Å^{-1} and then maximizing intensity/variance at $Q = 0.0020$ Å^{-1} while maintaining reasonable constraints. The resulting design is 48 m long, with a maximum wavelength band 16.8 Å $\leq \lambda \leq$ 20.5 Å.

The Monte Carlo simulations of instrument performance include wavelength-dependent effects from aluminum and fused silica windows, air, chopper opening and closing times and phase jitter, measured spectrum and detector efficiencies, sample transmission and multiple scattering, and gravity. The results were normalized by the measured flux from the present LANSCE moderator, and scaled by the expected performance of a coupled hydrogen moderator. The results compare well with the 76-m configuration of the D11 instrument at ILL in both count rate and Q-precision, due in part to the ability to correct for gravitation effects using the time of flight of the detected neutrons. The validity of these comparisons was demonstrated by comparison of measurements and Monte Carlo simulations made on the present LANSCE Low-Q instrument (LQD) and on D11.

Introduction

Neutron scattering with "small" momentum transfer gives information about the scattering system at "large" length scales: $Q = (4\pi \sin\theta)/\lambda \sim 1/d$ to $2\pi/d$. For example, determination of a radius of gyration R_g requires data for Q ? $1.3/R_g$. The technique of small-angle neutron scattering (SANS) also relies on use of long wavelengths to achieve low Q. Thus when performing measurements in the size range 300 Å or more, steady state (reactor) neutron sources with large cold moderators appear to have an advantage over spallation sources, whose spectra emphasize the epithermal regime. On the other hand, several successful SANS instruments have been built at spallation sources[1], and with careful attention to optimization of resolution[2,3] these instruments are

competitive with reactor SANS instruments over at least a portion of the "low-Q" range.

As part of the design study for a suite of instruments to be recommended for a proposed high-power pulsed neutron source, we were asked to consider the capability to measure length scales greater than 1000 Å, which are of particular interest in metallurgy, materials science, colloids, and polymers. To this end we chose to design a Very-Low-Q Diffractometer (VLQD) which would have comparable resolution to the 76-m configuration of D11 (D11-76) at the Institut Laue-Langevin[4]. Taking parameters for D11-76 from ref.[4], the collimation length is 40.5 m, sample-to-detector distance is 35.7 m, the maximum practical wavelength λ is 12 Å, and the minimum Q recorded is 0.00074 $Å^{-1}$.

In assessing the resolution of D11-76, we discovered that the effect of gravity is very deleterious. The velocity of a 12-Å neutron is 329.7 m/s, so the flight time is 0.234 s and the neutron falls 269 mm due to gravity. Parabolic trajectories defined as being on-axis at the entrance and exit of the collimation strike the detector below axis by an amount proportional to λ^2; specifically 0.84 λ^2 $mm/Å^2$. The resulting average droop of 121 mm is not in itself significant, but the variance of vertical position on the detector resulting from the spread of wavelengths of the velocity selector is the dominant term in the Q-resolution for any value of $Q \leq 0.002$ $Å^{-1}$. Thus the possibility to extend the Q range below about 0.002 $Å^{-1}$ is very limited at a steady-state source, because without knowledge of the velocity of each individual neutron there is no direct way to correct for the effect of gravity. A narrower velocity spectrum could be used, at the expense lowering the count rate below the already meager number available. In principle, image enhancement techniques could be applied to the data, but only if very high quality data are obtained.

At a pulsed source, on the other hand, it is trivial to correct for gravitational droop because the time of flight of each neutron *is* measured, and the droop is easily calculated. Therefore gravity does not limit the instrument length nor the wavelength range which may be used. We have designed the VLQD to operate on a 20-Hz , 330-kW target viewing a coupled liquid hydrogen moderator. Monte Carlo simulations of many geometries were tested, assuming a δ-function scatterer at $Q \equiv 0.0020$ $Å^{-1}$, and requiring a minimum recorded value of Q of 0.0007 $Å^{-1}$.

Instrument Geometry

Figure 1 illustrates the general instrument geometry which has been used in the design and analysis of a family of SANS instruments for the high-power source. The most significant variables are the total instrument length DT, the sample-to-detector distance L2, and the maximum wavelength λ_{max}; the search for an optimum is carried out over these three variables. Other elements which can be adjusted are the entrance aperture of the collimator (radius R1, located distance D1 from the moderator), the massive T_0 chopper (distance Dt from the moderator), the disk frame-definition chopper (distance Df from the moderator), the collimator exit aperture (radius R2, distance D2 from

moderator), and the beamstop. For the VLQD, we take D1 = 4.6 m, Dt = 5.0 m, Df = min{DT/2, DT −L2} − 1 m, D2 = DT − L2 − 0.15 m, and R1 and R2 determined by the cone rule[5] and the beam penumbra radius which results from computing the minimum scattering angle which must be measured to attain the required minimum Q. Similarly the nominal opening and closing times of the choppers are computed to assure closure during the initial pulse, and to give the maximum counting time without frame overlap. The T_0 chopper is two-lobed, rotating at half the proton pulse rate with an assumed phase jitter of 60 μs (rms), and the frame-definition chopper makes one revolution per proton pulse with phase jitter 30 μs (rms).

The detector is a very critical element in the performance of a SANS instrument, and we cannot give this presentation without stating very strongly our belief that detector development is the most crucial problem in improving existing instruments as well as being essential for instruments on a high-power neutron source, either pulsed or steady-state. The parameters of the detector which enter the Monte Carlo simulations are its overall size, the size of one pixel, the rms position encoding, the absorbing thickness of the entrance window, and the efficiency as a function of wavelength. We have assumed pixel size and rms to be similar to our existing ^{3}He detector (to facilitate comparison with actual measurements), but we hope for much larger area. (The simulations assume a detector 3 m wide by 1 m tall.) We have also retained the 1-cm Al entrance window, which greatly reduces efficiency at long wavelengths, and used the same gas fill pressure, which leads to lower efficiency at short wavelengths. Improved detectors will greatly affect our predicted instrument performance, but will probably not greatly affect the optimization procedure. In particular, elimination of the thick entrance window would vastly improve efficiency at the wavelengths we propose to use.

The effect of gravity in a long instrument with slow neutrons is that the trajectories have a high arch (proportional to λ^2) through the collimator. The intermediate baffles indicated in fig. 1 are not practical, so we are limited to a single-aperture collimation system instead of the multiple apertures shown. Also, the vertical motion required for the gravity focuser would be too large, so the VLQD is assumed not to have gravity focus. This means that all of the transmitted neutrons in the wavelength band of interest will droop *below* the beamstop, which will thus only intercept neutrons which scatter upward. We therefore plan to omit the beamstop in the VLQD; however since the wavelength bandpass is small, an adjustable beamstop could be included.

Monte Carlo Calculations

1. Neutron source

The direct spectrum of neutrons from the LANSCE liquid hydrogen moderator at 29 K was measured with a ^{3}He monitor detector of known efficiency at the sample position. The data were fitted by least squares with a semi-empirical function. This function was multiplied by λ^2, and integrated to give a cummulative probability distribution. A table of values of neutron energy was

generated such that the cummulative probabilities are the same as those of a normal distribution (truncated at ±3 σ). Then to find a random neutron energy from the distribution, we use a standard routine to generate a random normal deviate and interpolate in the table to get E. Note that because the distribution has been weighted by λ^2, more histories will be generated at the wavelengths which have higher scattering probability; each history is given an initial weight of $(\lambda_{max}/\lambda)^2$. This distribution accounts for absorption in the Al can of the cold moderator, but not the detector window.

After the neutron energy is determined, its emission time is selected from probability distributions including "slow" and "fast" components depending on wavelength. The parameters of the distributions are derived from early ISIS data; we have not felt the need to re-measure these distributions because the time spread is not a major contribution to SANS resolution.

2. Apertures and phase space

Only neutrons which pass through both apertures of the collimator need be tracked. We therefore begin by choosing a random point within each aperture, and projecting back (including the acceleration of gravity) to the moderator. Thus only a limited volume of phase space is sampled, namely $[\pi$ R1∃R2/(D2#D1)$]^2$ μster∃mm^2. Given the moderator surface brightness in neutrons/μ ster/mm^2/MW/s, the Monte Carlo results are normalized to MW∃s (or, in the case of a steady-state source, to s). Note that we have scaled the measured LANSCE source brightness upward by a factor of 4 for the expected gain of thermal flux from a strongly coupled moderator. Composite moderators may also be considered, which could have a similar gain.

3. Choppers

When a neutron track is projected to a chopper location, the location of the nearest moving edge is computed including a random normal deviate times the phase jitter. If the neutron position is on the closed side of the edge it is absorbed; otherwise it passes unaffected. Part of the program initialization is to set the nominal opening and closing times of the choppers to guarantee closure at T_0, including the time it takes to close fully and)3σ of jitter. The open duration of the frame-definition chopper is similarly set to give a maximum counting frame, and its phase is set to pass the requested λ_{max}.

4. Absorption in windows and air

A subroutine computes the aluminum scattering probability as a function of wavelength and compares it to a random number to decide whether the neutron was removed from the beam. The algorithm is taken from a note by Jack Carpenter[6], and explicitly includes Bragg edges up to the (820) reflection. Air and fused silica are treated simply by taking cross sections from the barn book[7].

5. Sample transmission and scattering

Sample thickness is expressed as transmission probability at λ_{max}, and is assumed to vary as $T(\lambda) = \exp(-\alpha \exists \lambda^2)$. When optimizing, $T(\lambda_{max})$ was arbitrarily set to 50%, but in comparisons with

D11 the sample thickness was kept constant such that transmission at 10 Å was always 75%. Every neutron history which strikes the sample is transmitted with its weight multiplied by $T(\lambda)$, and is also scattered with its initial weight multiplied by $[1 - T(\lambda)]$. The scattering law used to determine system performance is a δ-function; *i.e.*, every neutron scatters with exactly the same magnitude of Q, but the azimuthal angle is random. After the first scatter the probability of escaping the sample is computed by selecting a penetration depth from an exponential distribution, dividing the remaining thickness by the longitudinal direction cosine, and comparing the transmission probability to a random number. The scattering process is repeated until the neutron escapes.

6. Detector tallies

Transmitted neutrons and scattered neutrons that are still aimed downstream are projected to the plane of the detector (always including gravitational droop). If the X-Y position is within the physical bounds of the detector, encoding uncertainty is introduced by applying random normal deviates separately in X and Y, and the weight of the neutron is added to the corresponding X-Y-t cell. Time slices are logarithmic, defined using the algorithm of the LANSCE data acquisition system. At the completion of the Monte Carlo run, the X-Y-t data file is essentially identical to an LQD experiment, and is reduced to I(Q) using our standard procedures[8]. A typical result is shown in fig. 2. This figure also illustrates the effects of multiple, which is the only mechanism in the simulation which contributes to the "background" under the peak. These effects become severe whenever the sample transmission is low, as it was in this simulation.

7. Figure of merit (FOM)

A figure of merit (FOM) is needed to compare different configurations. The fundamental criterion is to maximize count rate at a given resolution, or equivalently to minimize the variance of Q at fixed count rate. The FOM is therefore I(Q)/V[Q]. We estimate scattered count rate by weighting the transmitted flux by λ^2 to account for variation of scattering probability. Because of the large number of terms which contribute to the δ-function response resolution in fig. 2, we can expect the shape to be Gaussian. We have estimated the variance V[Q] by fitting Gaussians to each of these plots. The units of the FOM as described are $Å^4/s$, but for comparing configurations at the same value of Q we normalize by multiplying by Q^4 so that the units are s^{-1}.

8. D11

As far as possible, the same code has been used to compute resolution and intensity at D11. One obvious difference is the neutron source function: the velocity selector is emulated by a triangular probability distribution with a full-width-half-maximum of 10%. There are no choppers and no gravity focuser, and time of flight is not recorded. When comparing optimum configurations the cone rule for collimator apertures is applied, but when comparing the real experiment the non-optimum practice of ILL is followed and there is no aperture at the guide exit.

Monte Carlo Results

After the first round of iteration on the three parameters (DT, L2, and λ_{max}), the proposed instrument was 46 m long, with L2 ≈ DT/2 (*cf.* fig. 3a) and $\lambda_{max} > 20$ Å (*cf.* fig. 3b). For the next series of simulations, λ_{max} was always adjusted (as DT was varied) so that the detector is never counting at the instant when protons are being delivered to the target; this will eliminate background problems associated with beam delivery and room background in the first 4 ms after each pulse. Note that the counting frame begins after three or four additional proton pulses have already been delivered to the target, so that there are four or five pulses in the instrument at any one time. The resulting plots of FOM *vs.* DT are given in fig. 3c. As usual, optimization leads to as long an instrument as possible. The selected design is 48 m long, and uses the counting frame from 204 to 249 ms after the proton pulse, corresponding to wavelengths from 16.8 to 25.6 Å. The frame-definition chopper (at 23.0 m) is open from 96.56 to 120.52 ms for each pulse, but its phase may also be adjusted to use shorter wavelength neutrons to extend the dynamic range in Q. The resulting resolution (at Q = 0.002 $Å^{-1}$) is 0.00031 $Å^{-1}$. The estimated integrated neutron flux on sample (area = 3.6 cm^2) is 1400 per second.

Figure 4 illustrates the Q-range and precision for the VLQD, compared to identical simulations of D11-76. (Three other pulsed-source instruments and three other D11 configurations are also shown.) The four lines represent setting the frame-definition chopper to count in the fifth, fourth, third, or second frames after T_0, while the box for D11 corresponds to varying the velocity selector between 12 Å and 6 Å. The resolution for VLQD frame 4 is identical to D11-76 for 10 Å neutrons, so it is appropriate to compare their intensities; see fig. 5. The computed VLQD intensity is a factor of 2.5 lower, but this is partly due to absorption of the long-wavelength neutrons in the detector window. With improved detectors, the intensity (for a 330 kW target) would be very comparable to D11-76. Thus these simulations show that a VLQD is completely feasible on the proposed high-power pulsed sources.

Code Validation

A comparison experiment between the present LQD and D11 at total lengths of 10 m and 20 m (sample-to-detector distances of 5 m and 10 m respectively) has previously been reported[1]. To test the validity of the Monte Carlo procedure, we have also simulated that experiment. The line labeled "LANSCE LQD" in fig. 4 shows our computed resolution. The value at Q = 0.020 $Å^{-1}$ (corresponding to the peak in the experiment) is 0.0023 $Å^{-1}$, while that computed for D11 at 10 m is 0.0020 $Å^{-1}$. This supports our statement in ref.[1] that the data for the two experiments are of the same quality. Furthermore the computed count-rate ratio is within 20% of the observed (which must be considered fortuitous), so that we can be reasonably confident in our comparisons.

Conclusions

The Monte Carlo calculations which are the basis of this report have proven to be extremely useful in understanding both existing and proposed future instruments. Each new feature added to the simulation seemed to produce an "ah-ha!" result – something obvious in retrospect but which we had previously overlooked. The first of these was the effect of gravity of steady-state sources which use long wavelength neutrons *and* long flight paths. Because droop is proportional to λ^2, the effect of the spread of wavelengths from a velocity selector is amplified. A second insight is that multiple-scattering effects can be extremely strong, and can lead to artifacts and high "incoherent" background even for scatterers which are purely coherent. For the simulatioin describing the comparison experiment, 30% of the detected neutrons were multiply scattered. We plan to use this simulation technique in the near future to study the possibility of correcting the experimental data.

Finally, and not surprising, the calculations again emphasize the need for detector development.

Acknowledgement

This work was performed at the Manuel Lujan Jr. Neutron Scattering Center (LANSCE), a national user facility operated by the US Department of Energy under contract W-7405-ENG-36 with the University of California.

References

1. P. A. Seeger and R. P. Hjelm Jr. (1991), "Small-Angle Neutron Scattering at Pulsed Spallation Sources," *J. Appl. Cryst.* **24**, 467-478.
2. P. A. Seeger and R. Pynn (1986), "Resolution of Pulsed-Source Small-Angle Neutron Scattering," *Nucl. Instrum. Methods* **A245**, 115-124.
3. R. P. Hjelm Jr. (1988), "The Resolution of TOF Low-Q Diffractometers: Instrumental, Data Acquisition and Reduction Factors," *J. Appl. Cryst.* **21**, 618-628.
4. P. Lindner, R. P. May and P. A. Timmins (1992), "Upgrading of the SANS Instrument D11 at the ILL," *Physica* **B 180&181**, 967-972.
5. P. A. Seeger (1980), "Optimization of Geometric Resolution in Small-Angle Scattering," *Nucl. Instrum. Methods* **178**, 157-161.
6. J. W. Carpenter (1986), "A Simple Formula for the Total Cross Section of a Monatomic Polycrystal," IPNS Note 32.
7. S. F. Mughabghab, M. Divadeenam and N. E. Holden, Neutron Cross Sections (Academic Press, New York, 1981).
8. R. P. Hjelm Jr. and P. A. Seeger (1988), "Time-of-Flight Small-Angle-Neutron-Scattering Data Reduction and Analysis at LANSCE with Program SMR," in Advanced Neutron Sources 1988, D. K. Hyer, ed., IOP Conference series **97** (Institute of Physics, Bristol and New York, 1989) pp 367-387.

Figure Captions

1. Generalized diagram of a Low-Q Diffraction instrument for a pulsed spallation neutron source. The nomenclature is discussed in the text. This arrangement has been used in the design of a family of diffractometers for a new high-power source.
2. Computed response function for a δ-function scatterer at $Q \equiv 0.0020$ Å^{-1}. The shape of the peak at $Q = 0.0020$ Å^{-1} gives the Q-resolution. The underlying background and the secondary structures are all results of multiple scattering. Data below $Q \approx 0.0007$ Å^{-1} have larger error bars because of subtraction of a background run including spreading of the direct beam.
3. Figure-of-Merit plotted *vs.* the three main parameters. a) variation of the secondary flight path with total length and wavelength held constant. b) variation of maximum wavelength with path lengths constant. c) variation of total instrument length with proportional changes in secondary path and wavelength.
4. Computed statistical resolution in Q as a function of Q for a number of SANS instruments. The various D11 configurations and the Biological LQD are shown as boxes representing continuous choices of wavelength. The present LQD and the proposed MQD record all wavelengths at a single setting, and the VLQD is expected to be operated at a few selected wavelengths.
5. Intensity of SANS instruments, weighted by λ^2. Only instruments with the same resolution on fig. 4 should be compared; *e.g.*, MQD and D11(11 m), Biology LQD and D11(21 m), or VLQD frame 4 and D11(76 m).

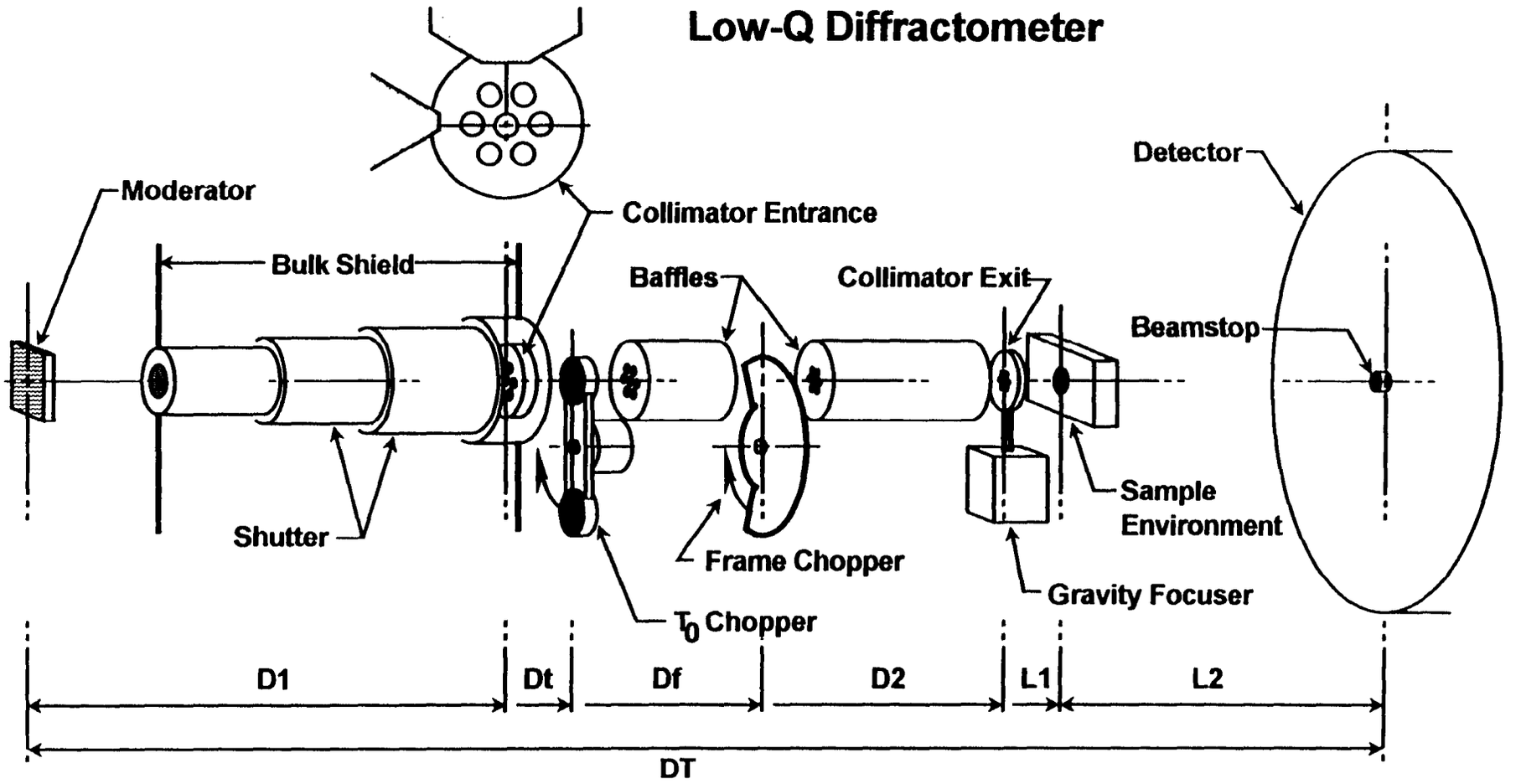
Low-Q Diffractometer
Moderator
Bulk Shield
Collimator Entrance
Baffles
Collimator Exit
Detector
Beamstop
Shutter
Frame Chopper
Sample Environment
Gravity Focuser
T0 Chopper
D1
Dt
Df
D2
L1
L2
DT

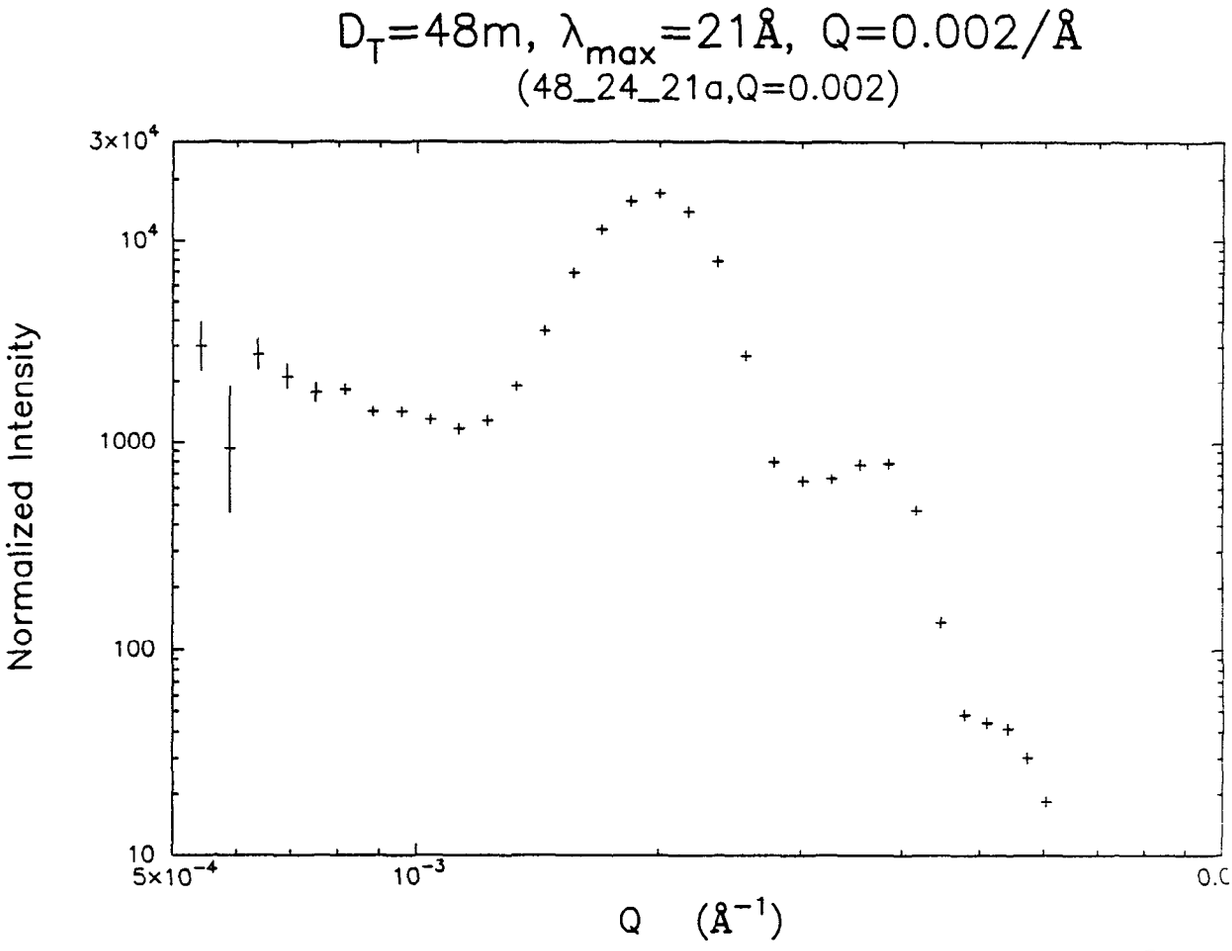
D_T=48m, λ_{max}=21Å, Q=0.002/Å
(48_24_21a,Q=0.002)
Normalized Intensity
3×10⁴
10⁴
1000
100
10
5×10⁻⁴
10⁻³
0.0
Q (Å⁻¹)

Fig.2

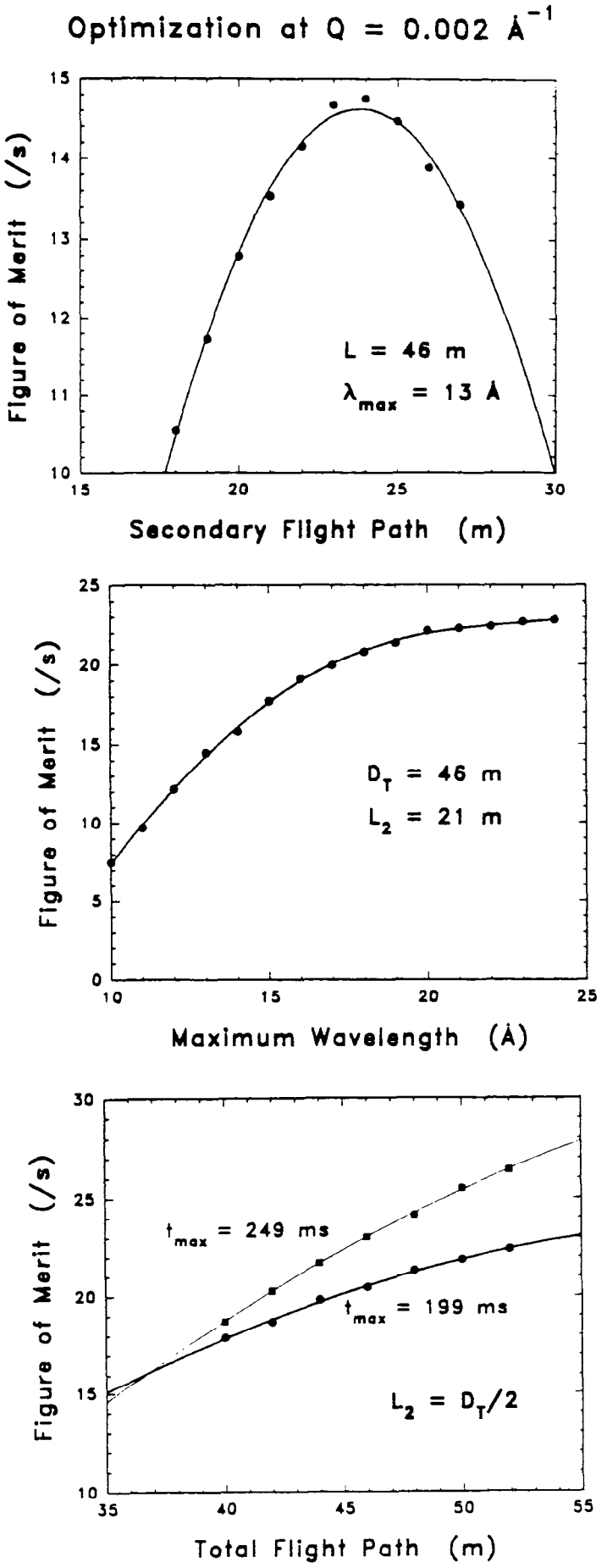
Optimization at Q = 0.002 Å^{-1}
Figure of Merit (/s)
Secondary Flight Path (m)
L = 46 m
λ_{max} = 13 Å
Figure of Merit (/s)
Maximum Wavelength (Å)
D_T = 46 m
L_2 = 21 m
Figure of Merit (/s)
Total Flight Path (m)
t_{max} = 249 ms
t_{max} = 199 ms
$L_2 = D_T/2$

Fig. 3

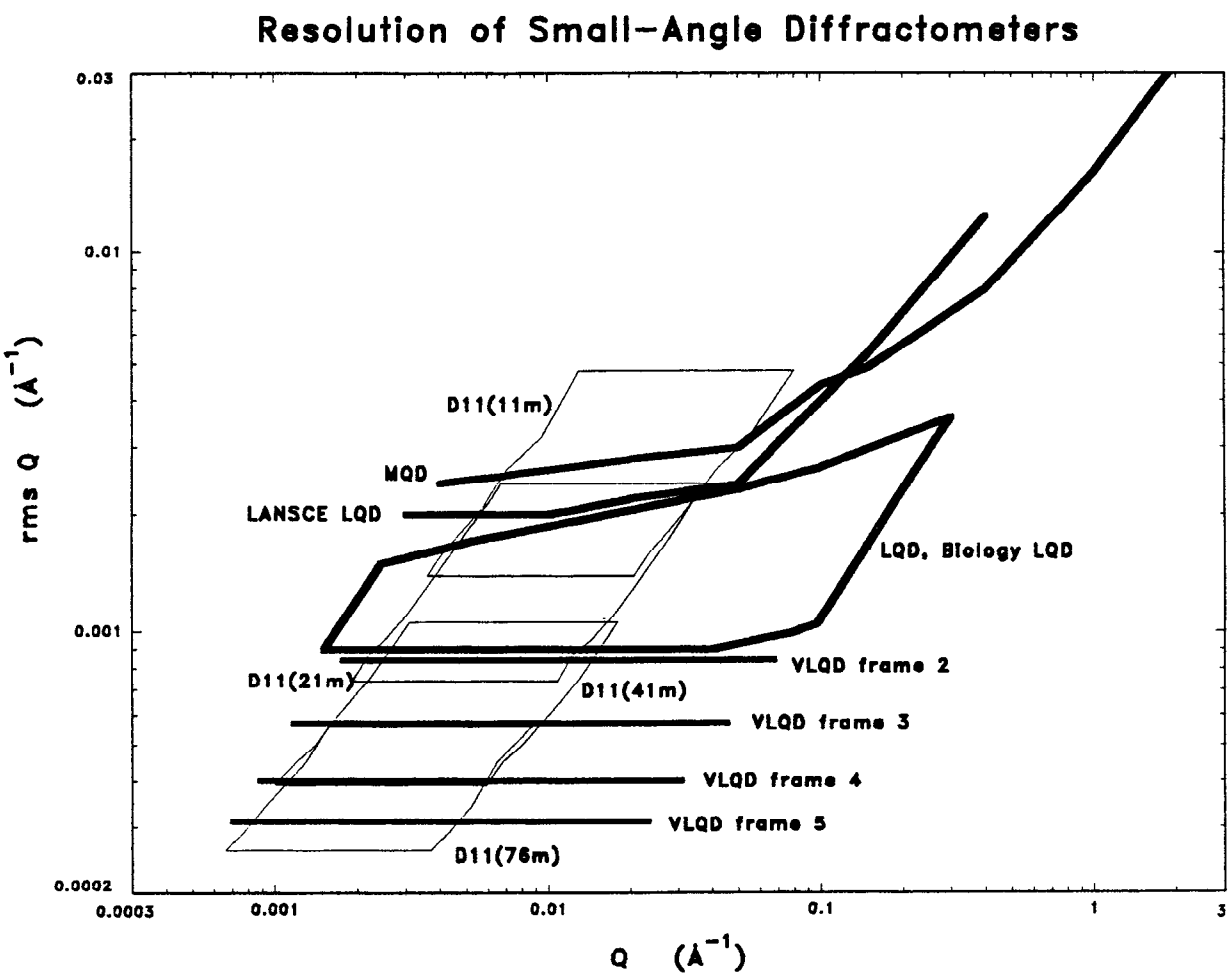
Resolution of Small-Angle Diffractometers
0.03
0.01
0.001
0.0002
rms Q (Å⁻¹)
0.0003
0.001
0.01
0.1
1
3
Q (Å⁻¹)
D11(11m)
MQD
LANSCE LQD
LQD, Biology LQD
VLQD frame 2
D11(21m)
D11(41m)
VLQD frame 3
VLQD frame 4
VLQD frame 5
D11(76m)

Fig. 4

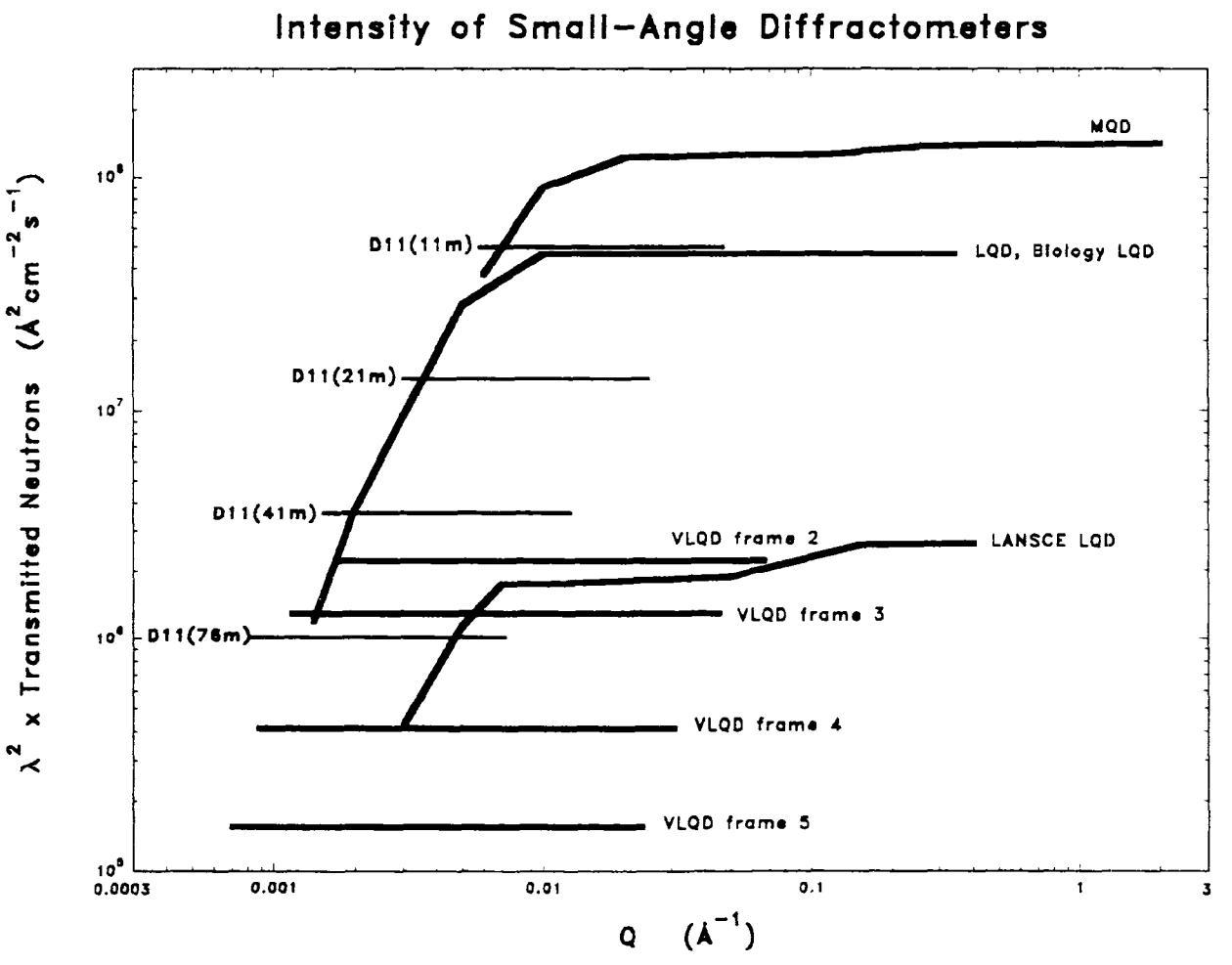
Intensity of Small-Angle Diffractometers
MQD
D11(11m)
LQD, Biology LQD
D11(21m)
D11(41m)
VLQD frame 2
LANSCE LQD
VLQD frame 3
D11(76m)
VLQD frame 4
VLQD frame 5
λ² x Transmitted Neutrons (Å² cm⁻² s⁻¹)
Q (Å⁻¹)
0.0003
0.001
0.01
0.1
1
3

Fig. 5